Journal of Ceramic Processing Research. Vol. 21, No. 1, pp. 5~13 (2020)
(Received 15 February 2019, Received in revised form 20 December 2019, Accepted 21 January 2020)
https://doi.org/10.36410/jcpr.2020.21.1.5

J O U R N A L O F
Ceramic Processing Research

Preparation of lead-free piezoelectric $(K_{0.5}Na_{0.5})NbO_3$ nanopowder by a simple aqueous route

John G. Fisher[a,*], Kwi-Hak Lee[a] and Won-Jin Moon[b]
[a]*School of Materials Science and Engineering, Chonnam National University, Gwangju 61186, Korea*
[b]*Korea Basic Science Institute, Gwangju Center, Gwangju 61186, Korea*

$(K_{0.5}Na_{0.5})NbO_3$-based ceramic powders for lead-free piezoelectric applications are usually prepared by solid state synthesis. This generally involves wet ball milling in an organic liquid such as ethanol, which is a drawback for industrial production. In the present work, a method for the preparation of $NaNbO_3$ nanopowders is modified to produce a simple method of preparing $(K_{0.5}Na_{0.5})NbO_3$ nanopowders by an aqueous route. K_2CO_3, Na_2CO_3 and $NH_4[NbO(C_2O_4)_2].xH_2O$ are mixed in water and dried to form a gel, which is then calcined at temperatures between 400 ~ 650 °C for 1 h. The uncalcined gel and calcination products are analysed using Thermogravimetric Analysis/Differential Thermal Analysis, X-ray Diffraction, Fourier Transform Infrared Spectroscopy, Scanning Electron Microscopy, Transmission Electron Microscopy and Raman Scattering. A single phase tetragonal $(K_{0.5}Na_{0.5})NbO_3$ nanopowder with a particle size of ~ 30 nm can be produced after calcination at 650 °C for 1 h.

Keywords: lead-free piezoelectric, $(K_{0.5}Na_{0.5})NbO_3$, nanopowder, microstructure.

Introduction

Materials based on $(K_{0.5}Na_{0.5})NbO_3$ (KNN) are leading contenders to replace lead-based piezoelectric ceramics such as $Pb(Zr,Ti)O_3$ and $Pb(Mn_{1/3}Nb_{2/3})O_3$-$PbTiO_3$ [1-7]. KNN-based powders are most commonly prepared by solid-state synthesis, in which alkali carbonates and Nb_2O_5 are mixed together by wet ball milling, followed by calcination at temperatures of 750 ~ 950 °C [3, 8-10]. Due to the hygroscopic and water-soluble nature of K_2CO_3 and Na_2CO_3, ethanol or acetone are usually used as the milling liquid [11, 12]. While use of organic solvents is acceptable in the laboratory, the use of organic solvents on an industrial scale increases production costs, as the solvents must be handled, recycled or disposed of according to local health and safety and environmental regulations [12]. In addition, KNN powders prepared by solid-state synthesis can suffer from chemical inhomogeneity which can cause variations in the electrical properties [10, 13, 14].

As a result, numerous studies have been carried out on the production of KNN powders by water-based methods such as the Pechini method, sol-gel combustion method, hydrothermal method, mechanochemical activation and spray-drying [15-31]. Besides avoiding the use of organic solvents, these processes have potential advantages such as lower synthesis or calcination temperatures, reduced powder size, narrow particle size distribution, improved chemical homogeneity and the possibility of forming nanostructures of different shapes such as nanowires, nanorods, nanocubes and microfingers.

The methods mentioned above can prepare KNN powders but often require specialized equipment or use complex chemical processes or corrosive chemicals. A simpler method which uses easily-handled chemicals would be beneficial. Su et al. described the synthesis of $NaNbO_3$ powders by simply mixing Na_2CO_3 and ammonium niobium oxalate, $NH_4[NbO(C_2O_4)_2(H_2O)_2](H_2O)_3$, in water to form a slurry, followed by drying and calcination at different temperatures [32]. A single phase $NaNbO_3$ nanopowder could be formed at a calcination temperature as low as 400 °C. In the present work, their method is modified to produce nanopowders of $(K_{0.5}Na_{0.5})NbO_3$.

Experimental

K_2CO_3 (Alfa Aesar, 99%), Na_2CO_3 (Acros Organics, 99.5%) and ammonium niobium oxalate $NH_4[NbO(C_2O_4)_2].xH_2O$ (Aldrich, 99.99%) were used as starting materials. The mass% of Nb_2O_5 in the $NH_4[NbO(C_2O_4)_2].xH_2O$ powder was determined by Thermogravimetric Analysis/Differential Thermal Analysis (TG/DTA, DTG-60, Shimadzu, Kyoto, Japan). The K_2CO_3 and Na_2CO_3 powders were dried at 250 °C for 2 h before weighing to remove adsorbed water. The $NH_4[NbO(C_2O_4)_2]\cdot xH_2O$ powder was not dried. Stoichiometric amounts of the starting materials (enough to make 5 g of $(K_{0.5}Na_{0.5})NbO_3$ powder) were weighed and dissolved

*Corresponding author:
Tel : +82-62-530-1702
Fax: +82-62-530-1699
E-mail: johnfisher@jnu.ac.kr

in 100 ml of deionized water. The solution was stirred using a digital hotplate/magnetic stirrer (MaXtir 500, Daihan, Wonju, Korea) at a temperature of 65 °C and a rotation speed of 250 rpm for 1 h. The solution temperature was controlled using a temperature probe inserted in the solution. The temperature was then increased to 95 °C and the solution evaporated until ~25 vol% remained. The remaining solution was heated at 200 °C for 3 h. The solution transformed into a white porous gel. After cooling, the gel was crushed into powder in an agate mortar and pestle.

Thermogravimetric Analysis/Differential Thermal Analysis (TG/DTA, DTG-60, Shimadzu, Kyoto, Japan) was carried out on the $NH_4[NbO(C_2O_4)_2]\cdot xH_2O$ powder and gel powder in the temperature range 25 ~ 1000 °C in air at a heating rate of 10 °C·min^{-1}. Samples of gel powder were calcined at temperatures of 400, 450, 500, 550, 600 and 650 °C for 1 h in air with heating and cooling rates of 5 °C·min^{-1}. X-ray Diffraction (XRD) was carried out on uncalcined and calcined samples with Cu Kα radiation (XRD XPert PRO, PANalytical, The Netherlands) with 2θ range = 20° ~ 80°, scan speed = 3°·min^{-1} and 0.02° step size. Fourier Transform Infrared spectroscopy was carried out on the starting materials, uncalcined gel powder and calcined samples (FTIR, Spectrum 400, Perkin Elmer, Waltham, MA). Powder samples were mixed with KBr and pressed into pellets. Scanning Electron Microscopy (SEM, Hitachi S-4700, Tokyo, Japan) was carried out on uncalcined and calcined samples. Raman scattering (LabRam HR800 UV Raman microscope, Horiba Jobin-Yvon, France), with a 515 nm diode laser and output power of 10 mW, was carried out on a powder sample calcined at 650 °C for 1 h. Spectra were recorded in back scattering geometry over a range of 50 ~ 1,000 cm^{-1} with a resolution of ~ 0.5 cm^{-1}.

In order to study the structure in more detail, XRD (D8 Advance, Bruker, Billerica, MA) with Cu Kα radiation, 2θ range = 20° - 80°, scan speed = 0.3°·min^{-1} and 0.0062° step size was carried out on a powder sample calcined at 650 °C for 1 h. A powder sample calcined at 650 °C for 1 h was also studied using Transmission Electron Microscopy (TEM, FEI TECNAI F 20, FEI Company, Hillsboro, OR) operated at an accelerating voltage of 200 kV.

Results and Discussion

A TG/DTA trace of the precursor $NH_4[NbO(C_2O_4)_2]\cdot xH_2O$ powder is shown in Fig. 1. The DTA trace contains endothermic peaks at 129 °C, 183 °C and 258 °C (with a shoulder at 275 °C), and an exothermic peak at 596 °C (with a shoulder at 579 °C). The peak at 129 °C corresponds to the loss of water of hydration and is accompanied by a loss in weight of ~ 10%. The endothermic peaks at 183 °C and 258 °C correspond to the release of NH_3 and the decomposition of the organic material in $NH_4[NbO(C_2O_4)_2]\cdot xH_2O$ as it transforms to amorphous niobic acid $Nb_2O_5\cdot nH_2O$ [32-35]. These peaks are accompanied by a weight loss of ~ 55%. The exothermic peak at 596 °C corresponds to the crystallisation of amorphous niobic acid into a hexagonal or orthorhombic phase [33, 34, 36, 37]. The small accompanying weight loss of ~ 4% may be due to the release of CO_2 caused by oxidation of residual carbon [33]. A total weight loss of 70.3% was measured between 25 ~ 1,000 °C.

A TG/DTA trace of the uncalcined gel is shown in Fig. 2. The sample has a broad endothermic peak at 100 °C, accompanied by a weight loss of ~ 3.8% which corresponds to the loss of water of hydration. A large endothermic peak at 257 °C followed by a smaller peak at 361 °C corresponds to the decomposition of the gel into K_2CO_3, Na_2CO_3 and $Nb_2O_5\cdot nH_2O$ [27, 32]. These peaks are accompanied by a weight loss of ~ 47.8%. Exothermic peaks at 490 °C and 535 °C correspond to the decomposition of the K_2CO_3 and Na_2CO_3 and the reaction to form $(K_{0.5}Na_{0.5})NbO_3$ [27, 38, 39]. These peaks are accompanied by a weight loss of ~ 2.5%. A further small weight loss may be due to the decomposition

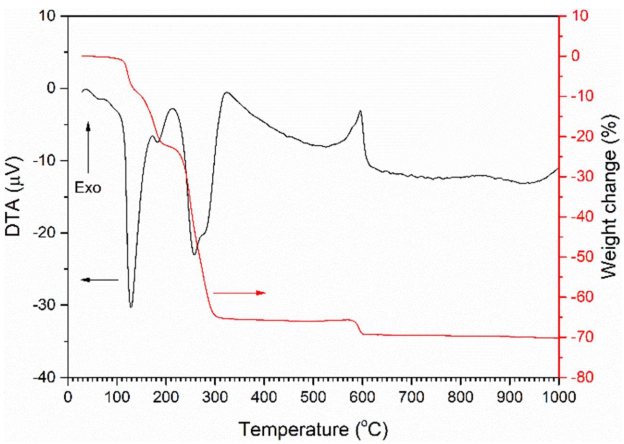

Fig. 1. TG/DTA trace of $NH_4[NbO(C_2O_4)_2]\cdot xH_2O$ powder.

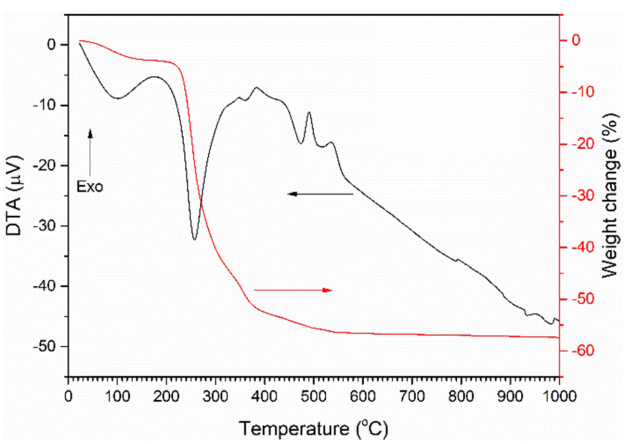

Fig. 2. TG/DTA trace of uncalcined gel.

of unreacted K_2CO_3 and Na_2CO_3. Total weight loss is 57.3%.

Fig. 3(a) shows an XRD pattern of the uncalcined gel. The gel has an amorphous structure. An FTIR spectrum of the precursor $NH_4[NbO(C_2O_4)_2].xH_2O$ powder is shown in Fig. 3(b). The main infrared bands are summarized in Table 1 [33, 34, 40]. An FTIR spectrum of the uncalcined gel is shown in Fig. 3(c). The main infrared bands are summarized in Table 2 [33, 34, 41]. Shifts in the peak positions and the absence of the main K_2CO_3 and Na_2CO_3 peaks at 1,450 cm^{-1} indicate that $NH_4[NbO(C_2O_4)_2]\cdot xH_2O$ has reacted with K_2CO_3 and Na_2CO_3 to form a gel [41]. However, the appearance of new peaks at 1,259 and 907 cm^{-1} due to the ligand exchange reaction between H_2O and NH_3 was not observed [32]. In addition to the bands from $NH_4[NbO(C_2O_4)_2].xH_2O$, bands from the carbonate groups of K_2CO_3 and Na_2CO_3 are present at 703 and 860 cm^{-1}, indicating that not all of the K_2CO_3 and Na_2CO_3 has reacted with the $NH_4[NbO(C_2O_4)_2].xH_2O$.

XRD patterns of the gel calcined at temperatures between 400 ~ 650 °C for 1 h are shown in Fig. 4. Also included are the patterns for ICDD card #77-0038 [$(Na_{0.35}K_{0.65})NbO_3$, monoclinic, space group Pm(6)], ICDD card # 74-2449 [$NaNbO_3$, monoclinic, space group P2/m(10)] and ICDD card #76-0977 [$K_4Nb_6O_{17}$, orthorhombic, space group P21nb(33)]. After calcination at 400 °C, the sample appears to be still amorphous. As the calcination temperature increases to 450 °C, very broad peaks corresponding to $(K_{0.5}Na_{0.5})NbO_3$, $NaNbO_3$ and $K_4Nb_6O_{17}$ form. As the calcination temperature

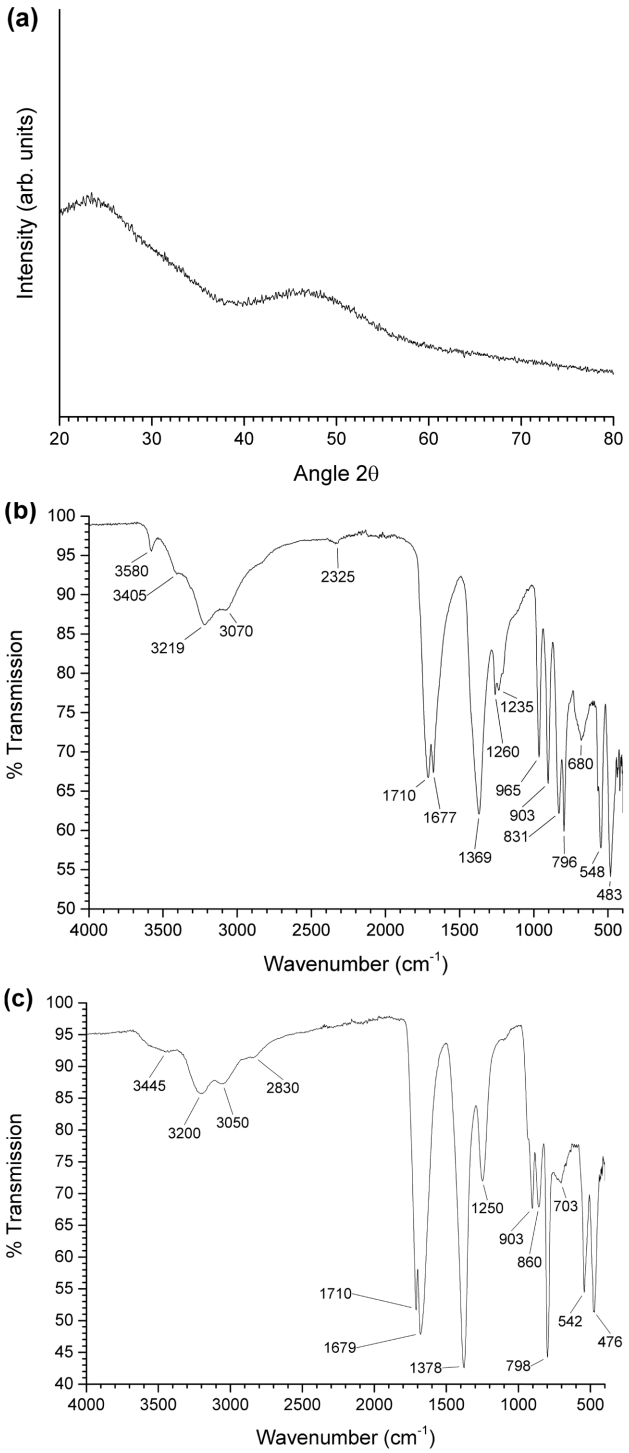

Fig. 3. (a) XRD pattern of uncalcined gel; (b) FTIR spectrum of $NH_4[NbO(C_2O_4)_2].xH_2O$ powder; (c) FTIR spectrum of uncalcined gel.

Table 1. Infrared bands of $NH_4[NbO(C_2O_4)_2].xH_2O$.

Bands (cm^{-1})	Assignment
483, 548	$\nu_{Nb\text{-}O}$
680	Unknown
796	$\delta_{(COO)^-}$
831	Unknown
903, 965	$\nu_{Nb=O}$
1235, 1260	$\nu_{C\text{-}O}$
1369	$\delta_{N\text{-}H}$, $\nu_{C=O}$, $\nu_{C\text{-}C}$
1677	$\delta_{O\text{-}H}$, $\nu_{C=O}$
1710	$\nu_{C=O}$
2325	$\nu_{C\text{-}H}$
3070, 3219	$\nu_{N\text{-}H}$, $\nu_{O\text{-}H}$
3405, 3580	$\nu_{O\text{-}H}$

Table 2. Infrared bands of the uncalcined gel.

Bands (cm^{-1})	Assignment
476, 542	$\nu_{Nb\text{-}O}$
703	$\nu_{CO_3^{2-}}$
798	$\delta_{(COO)^-}$
860	$\nu_{CO_3^{2-}}$
903	$\nu_{Nb=O}$
1250	$\nu_{C\text{-}O}$
1378	$\delta_{N\text{-}H}$, $\nu_{C=O}$, $\nu_{C\text{-}C}$
1679	$\delta_{O\text{-}H}$
1710	$\nu_{C=O}$
2830	Unknown
3050, 3200	$\nu_{N\text{-}H}$
3445	$\nu_{O\text{-}H}$

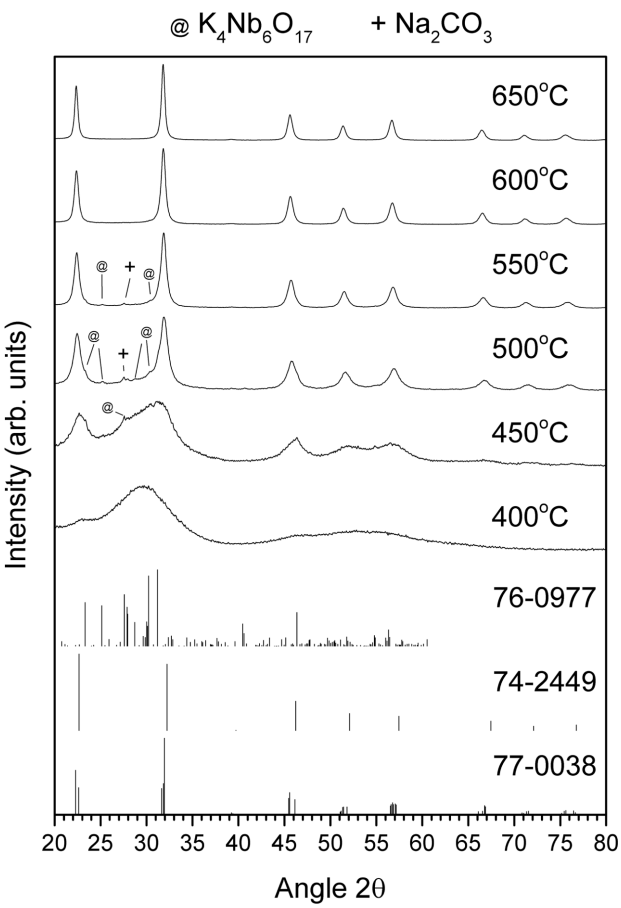

Fig. 4. XRD patterns of gel calcined at temperatures between 400 ~ 650 °C for 1 h.

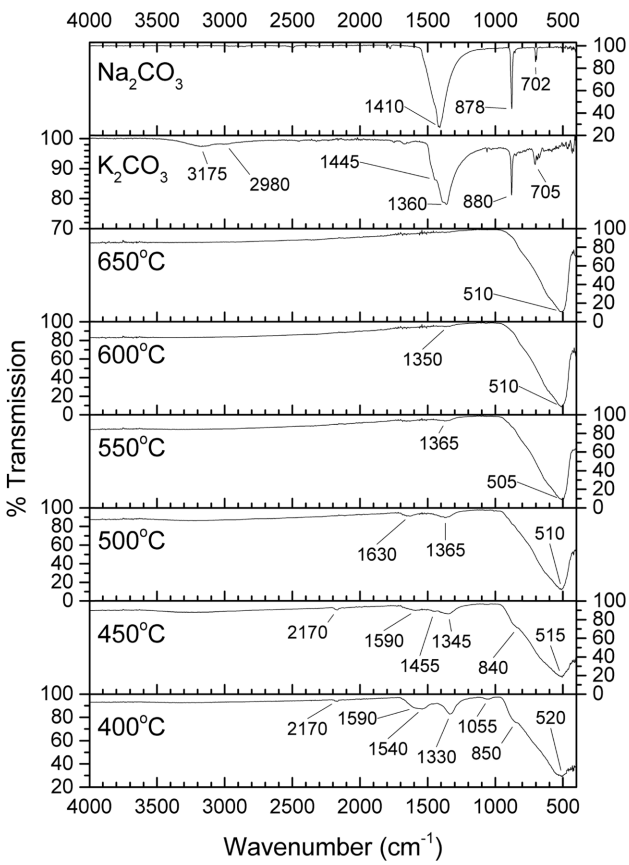

Fig. 5. FTIR spectra of gel calcined at temperatures between 400 ~ 650 °C for 1 h.

increases from 450 to 500 °C, the peaks become narrower and better defined. The peaks corresponding to $NaNbO_3$ shift to smaller values of 2θ and merge with the peaks corresponding to $(K_{0.5}Na_{0.5})NbO_3$. As the calcination temperature increases from 450 °C, the peaks corresponding to $K_4Nb_6O_{17}$ gradually decrease in intensity, finally disappearing at 600 °C. Some unreacted Na_2CO_3 is also present in the samples calcined at 500 °C and 550 °C (ICDD card # 86-0309).

The crystallite size of the sample calcined at 650 °C for 1 h was estimated using Scherrer's formula:

$$\tau = \frac{0.9\lambda}{\beta\cos\theta} \tag{1}$$

where τ = crystallite size, λ = X-ray wavelength (0.154184 nm for Cu Kα), β = FWHM (in radians) and θ = Bragg angle. Using the (200) peak with $\theta = 11.16°$, the crystallite size was estimated to be 20 nm.

FTIR spectra of the gel calcined at temperatures between 400 °C - 650 °C for 1 h are shown in Fig. 5. FTIR spectra of the K_2CO_3 and Na_2CO_3 precursor powders are also included. A comparison of the spectra of the uncalcined gel and the sample calcined at 400 °C clearly show that the gel has decomposed. The peaks at 520 and 850 cm^{-1} in the sample calcined at 400 °C are due to Nb-O vibrations [33, 42]. The peak at 1,330 cm^{-1} in the sample calcined at 400 °C may belong to a CH_3 bending mode [16] or to an oxalate group such as $Na_2C_2O_4$ or $K_2C_2O_4$ [43, 44]. It should be noted that the gel calcined at 400 °C contains partially decomposed organic material and is black in colour. The peaks at 1,330 cm^{-1}, 1,540 cm^{-1} and 1,590 cm^{-1} may also belong to a carbonato complex [45, 46]. The band at 1,055 cm^{-1} may correspond to a C-OH stretching vibration or to the ν_1 vibration of the carbonate ion [16, 45, 47]. The ν_1 vibration is usually infrared inactive, but becomes active when the coordination symmetry of the carbonate ion is lowered i.e. the crystal structure of the carbonate is degraded. These peaks therefore indicate the decomposition of the gel and the formation of alkali carbonates. As the calcination temperature increases to 500 °C, these peaks change position and gradually disappear, while peaks associated with Na_2CO_3 (1,455 cm^{-1}) and K_2CO_3 (1,455 cm^{-1}, 1,365 cm^{-1}, 1,630 cm^{-1}) appear. These peaks belong to unreacted alkali carbonates. As the calcination temperature increases further, the peaks associated with the alkali carbonates also decrease, finally disappearing in the sample calcined at 650 °C. The colour of the calcined samples also becomes lighter with calcination temperature, finally

becoming white at 650 °C. Changes in the position and width of the peaks at 520 and 850 cm^{-1} as the calcination temperature increases indicate the formation of $(K_{0.5}Na_{0.5})NbO_3$.

An SEM micrograph of the uncalcined gel is shown in Fig. 6(a). The gel has a honeycomb appearance, which may be caused by the release of NH_3 and CO_2 during the ion exchange reaction between the starting materials. A micrograph taken at higher magnification shows that the gel appears to lack any polycrystalline structure [Fig. 6(b)]. An SEM micrograph of the gel after calcination at 650 °C for 1 h shows that the calcined gel maintains the honeycomb structure [Fig. 6(c)]. The samples calcined at lower temperatures look similar.

High magnification SEM micrographs of the gel after calcination at different temperatures for 1 h are shown in Fig. 7. All the samples show a polycrystalline microstructure consisting of nano-sized grains, even the sample calcined at 400 °C. The grain size coarsens slightly as calcination temperature increases, but even after calcination at 650 °C, the mean grain size is only ~ 30 nm. This agrees quite well with the estimation of crystallite size using Scherrer's formula. The samples calcined at temperatures ≥ 500 °C show some areas with abnormal coarsening, with some grains up to 100 nm in diameter. The nano-sized grains have partially sintered together to form agglomerates, even after calcination at the low temperature of 400 °C. The small grain radius and high surface area provides a high driving force for sintering, causing the grains to partially sinter together during the calcination process [48, 49]. The agglomerate size may be reduced by ball milling [50] or by cold isostatic pressing of the powder to break the agglomerates [51].

A slow-scan XRD pattern of a gel sample calcined at 650 °C for 1 h is shown in Fig. 8. The pattern can be

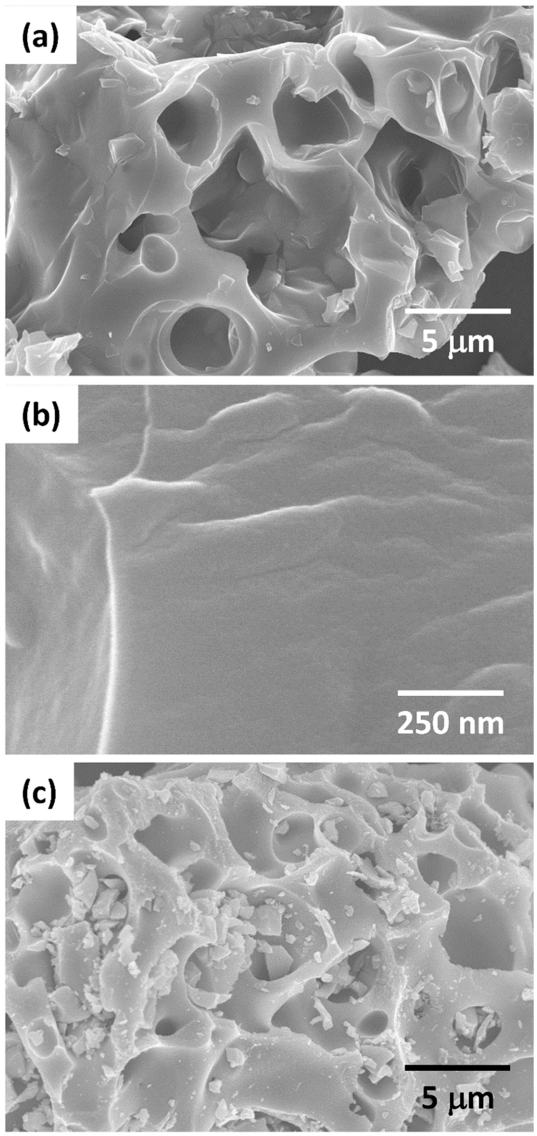

Fig. 6. (a) and (b) SEM micrographs of uncalcined gel; (c) SEM micrograph of gel calcined at 650 °C for 1 h.

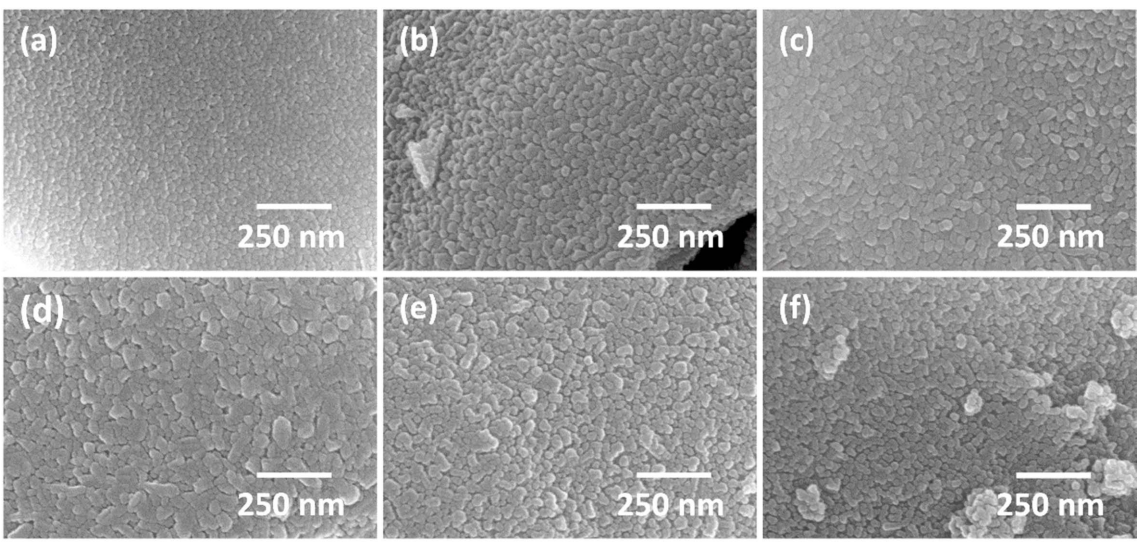

Fig. 7. SEM micrographs of gel calcined for 1 h at (a) 400 °C, (b) 450 °C, (c) 500 °C, (d) 550 °C, (e) 600 °C and (f) 650 °C.

indexed with ICDD card# 71-0948 ($KNbO_3$, tetragonal, space group P4mm). The unit cell parameters were refined as a = 3.9528 Å, c = 4.0033 Å. $(K_{0.5}Na_{0.5})NbO_3$ usually has an orthorhombic unit cell at room temperature. The change in symmetry to tetragonal is caused by the very small grain size [52]. A small peak at 28.5° (marked with an asterisk) may be due to unreacted K_2CO_3 (ICDD card # 87-0730) or to $K_3Nb_7O_{19}$ (ICDD card # 84-0812).

TEM micrographs of a gel sample calcined at 650 °C for 1 h are shown in Fig. 9(a) and Fig. 9(d). The grains are cubic in shape, as is typical for $(K_{0.5}Na_{0.5})NbO_3$ [10, 53] and vary in size from 20-200 nm. It can clearly be seen that the nano-sized grains have sintered together to form agglomerates. Fig. 9(b) shows a high-resolution TEM image of the grain marked by an arrow in Fig. 9(a). The crystal structure of the grain can clearly be seen. Fig. 9(c) shows a selected area diffraction pattern of a different grain. The pattern was indexed using a tetragonal unit cell. EDS point analysis of the three grains marked in Fig. 9(d) is shown in Table 3. The chemical compositions of the grains are close to the nominal composition for $(K_{0.5}Na_{0.5})NbO_3$, indicating good chemical homogeneity of the powder.

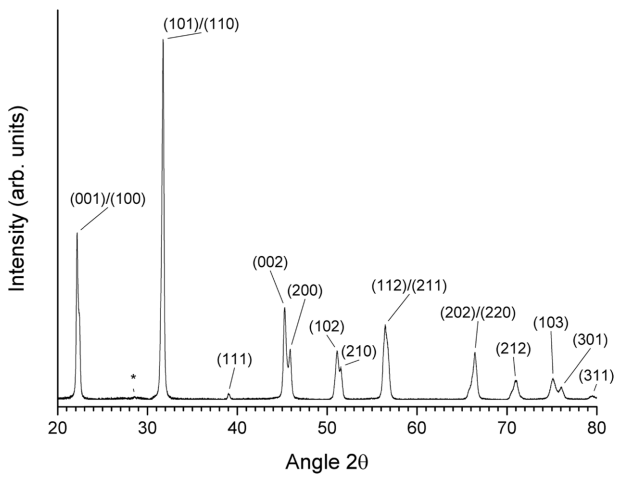

Fig. 8. Slow-scan XRD pattern of gel calcined for 1 h at 650 °C.

A Raman spectrum of a gel sample calcined at 650 °C for 1 h is shown in Fig. 10. The spectrum shows features typical of $(K_{0.5}Na_{0.5})NbO_3$ [54, 55]. The peak at 85 cm^{-1} and the shoulder at 190 cm^{-1} are assigned to translational modes of Na^+/K^+ cations and rotations of the NbO_6 octahedra. The peak at 260 cm^{-1} is assigned to the ν_5 NbO_6 bending mode. The shoulder

Table 3. TEM-EDS point analysis of gel calcined for 1 h at 650 °C [Fig. 9(d)].

Element	Composition Point 1 (at.%)	Composition Point 2 (at.%)	Composition Point 3 (at.%)	Nominal composition (at.%)
K	11.23	11.94	13.86	10
Na	11.56	14.02	13.4	10
Nb	23.25	23.44	25.85	20
O	53.94	50.58	46.87	60

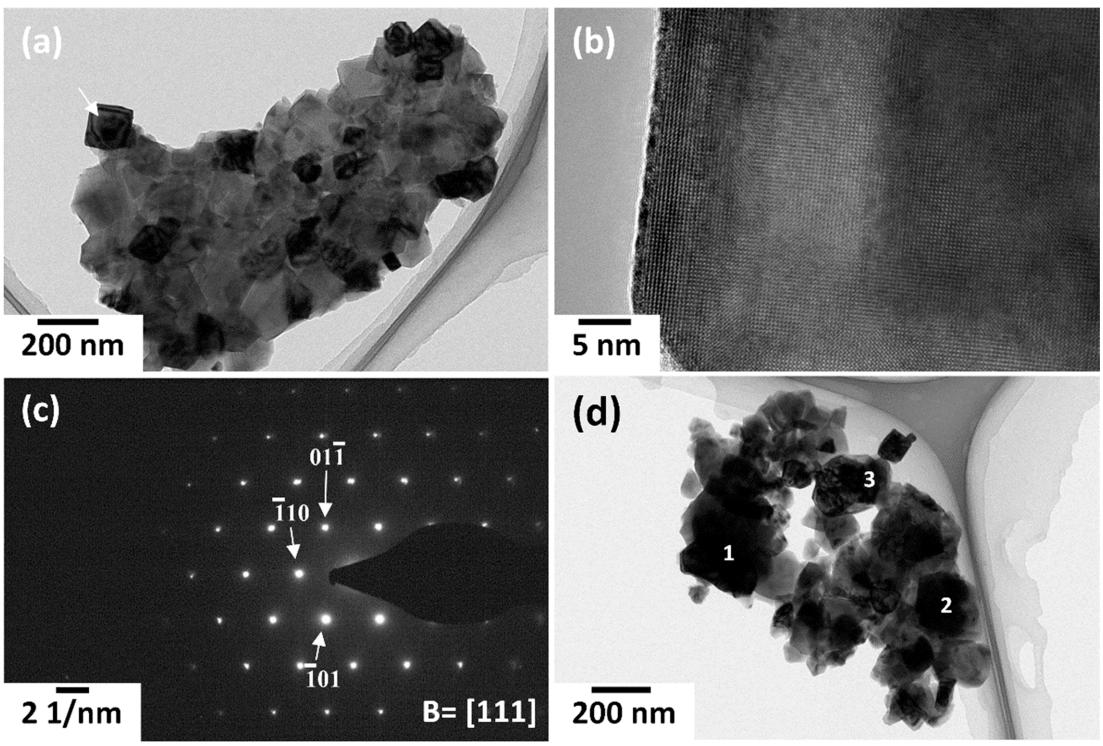

Fig. 9. (a), (d) TEM micrographs of gel calcined for 1 h at 650 °C; (b) HRTEM micrograph of the grain marked by an arrow in (a); (c) SADP of a grain.

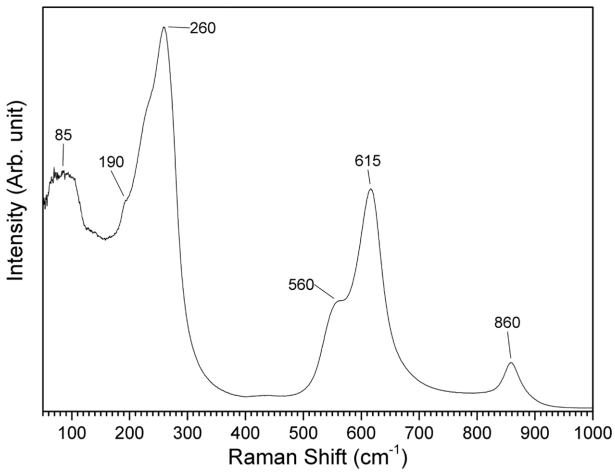

Fig. 10. Raman spectrum of gel calcined for 1 h at 650 °C.

at 560 cm^{-1} and the peak at 615 cm^{-1} are assigned to the v_2 and v_1 NbO_6 stretching modes respectively. At 860 cm^{-1}, there is a mode assigned to a combination tone of the v_1 and v_5 modes. The overlap of the v_1 and v_2 modes may indicate the tetragonal phase of $(K_{0.5}Na_{0.5})NbO_3$ [56].

According to Su et al., the following ion exchange reaction takes place between alkali carbonates and ammonium niobium oxalate [32]:

$$2NH_4[NbO(C_2O_4)_2(H_2O)_2](H_2O)_3 + A_2CO_3 \rightarrow 2A[NbO(C_2O_4)_2(H_2O)_2](H_2O)_3 + 2NH_3 + CO_2 + H_2O \quad (A = K, Na) \qquad (2)$$

This is then followed by a ligand exchange reaction:

$$A[NbO(C_2O_4)_2(H_2O)_2](H_2O)_3 + 2NH_3 \rightarrow A[NbO(C_2O_4)_2(NH_3)_2](H_2O)_3 + 2H_2O \qquad (3)$$

Only half of the oxalate will undergo the ligand exchange reaction due to an insufficient amount of ammonia. Upon heating, the gel decomposes into K_2CO_3, Na_2CO_3 and $Nb_2O_5{\cdot}nH_2O$ according to the following reactions:

$$2A[NbO(C_2O_4)_2(H_2O)_2](H_2O)_3 + 2O_2 \rightarrow A_2CO_3 + Nb_2O_5{\cdot}nH_2O + 7CO_2 + (10 - n)H_2O \qquad (4)$$

$$2A[NbO(C_2O_4)_2(NH_3)_2](H_2O)_3 + 2O_2 \rightarrow A_2CO_3 + Nb_2O_5{\cdot}nH_2O + 7CO_2 + 4NH_3 + (6 - n)H_2O \qquad (5)$$

Because the alkali ions and niobium ions are mixed in the gel on a molecular scale, the gel decomposes to give a finely interspersed mixture of alkali carbonates and $Nb_2O_5{\cdot}nH_2O$. This reduces the diffusion distances needed for subsequent chemical reactions, allowing the $(K_{0.5}Na_{0.5})NbO_3$ phase to be formed at lower calcination temperatures than those achieved by conventional solid state processing. The higher reactivity of $Nb_2O_5{\cdot}nH_2O$ compared to Nb_2O_5 is also beneficial. In the present work, single phase $(K_{0.5}Na_{0.5})NbO_3$ nanopowders could be formed at calcination temperatures comparable to those of other aqueous preparation methods, but with a much simpler process [16, 18, 26].

In their work, Su et al. were able to prepare single phase $NaNbO_3$ powders using calcination temperatures as low as 400 °C [32]. However, in the present work a calcination temperature of 600 °C was necessary to obtain a single phase powder. Furthermore, the $(K_{0.5}Na_{0.5})NbO_3$ phase appears to develop via intermediate $NaNbO_3$ and $K_4Nb_6O_{17}$ phases. It should be noted that, as well as the $NaNbO_3$ phase, there are other $(K_{1-x}Na_x)NbO_3$ phases with very similar diffraction patterns to $NaNbO_3$ and $(K_{0.5}Na_{0.5})NbO_3$ (ICDD card # 74-2024 for $(K_{0.02}Na_{0.98})NbO_3$ and ICDD card #s 74-2025 and 77-0037 for $(K_{0.1}Na_{0.9})NbO_3$) and it is difficult to assign particular diffraction patterns to the XRD traces as $KNbO_3$ and $NaNbO_3$ form a complete range of solid solutions [57]. On calcination at 400 and 450 °C, the gel powder probably forms a range of sodium-rich $(K_{1-x}Na_x)NbO_3$ phases along with $K_4Nb_6O_{17}$ and as the calcination temperature increases, the overall composition moves towards $(K_{0.5}Na_{0.5})NbO_3$. The exact nature of the sample after calcination at 400 °C is not known. From the XRD pattern (Fig. 4) it appears amorphous, but from the SEM micrograph it appears polycrystalline (Fig. 7). The sample may be partially crystalline.

Malic et al. studied the synthesis of $(K_{0.5}Na_{0.5})NbO_3$ from alkali carbonates and Nb_2O_5 by the use of diffusion couples of K_2CO_3/Nb_2O_5, Na_2CO_3/Nb_2O_5 and $(K_2CO_3+Na_2CO_3)/Nb_2O_5$ [58]. They found that the perovskite phase formed via intermediate phases such as $Na_2Nb_4O_{11}$, $K_6Nb_{10.88}O_{30}$, $K_4Nb_6O_{17}$ and $(K,Na)_2Nb_4O_{11}$. They also found that the reaction rate for formation of $(K_{0.5}Na_{0.5})NbO_3$ was determined by the diffusion of the more slowly moving K^+ ions and that the reaction rate constant for the reaction in the K_2CO_3/Nb_2O_5 and $(K_2CO_3+Na_2CO_3)/Nb_2O_5$ diffusion couples was an order of magnitude slower than that of the Na_2CO_3/Nb_2O_5 diffusion couple.

Yang et al. in their synthesis of $(K_{0.5}Na_{0.5})NbO_3$ powders by the Polymerized Complex method found that $(K_{0.5}Na_{0.5})NbO_3$ formed via intermediate $NaNbO_3$ and $K_2Nb_8O_{21}$ phases [15]. Similar results were found in the synthesis of KNN powders by the hydrothermal method [17, 21] Toyama et al. in their study of the synthesis of $(K_{1-x}Na_x)NbO_3$ nanoparticles using a supercritical water flow system also found that $KNbO_3$ could form via an intermediate $K_4Nb_6O_{17}$ phase [24]. $NaNbO_3$, on the other hand, formed directly and $(K_{1-x}Na_x)NbO_3$ nanoparticles always had a higher Na/K molar ratio than the molar ratio of the starting precursors, indicating that Na^+ ions have a higher reactivity than K^+ ions. This difference in diffusion rates and reactivity of the alkali ions would explain why intermediate phases form and why a higher calcination temperature then that of Su et al. is needed to obtain a single phase $(K_{0.5}Na_{0.5})NbO_3$ powder in the present work. Sodium-

rich $(K_{1-x}Na_x)NbO_3$ phases form first due to the higher diffusion rate and reactivity of the Na^+ ions. These phases then change to the $(K_{0.5}Na_{0.5})NbO_3$ composition at higher calcination temperatures due to the increase in diffusion rate and reactivity of K^+ ions.

Conclusions

Based on the work of Su et al., a facile aqueous method for the production of $(K_{0.5}Na_{0.5})NbO_3$ nanopowders from alkali carbonates and ammonium niobium oxalate has been developed. The alkali carbonates and ammonium niobium oxalate are dissolved and mixed in water and an ion exchange reaction takes place between the ammonium niobium oxalate and alkali carbonates. The water is then evaporated, leaving behind a gel which is then calcined. From the TG/DTA, XRD and FTIR results, the calcination reactions begin at temperatures between 450-500 °C, but a calcination temperature of 650 °C is needed to form a single phase $(K_{0.5}Na_{0.5})NbO_3$ powder. The $(K_{0.5}Na_{0.5})NbO_3$ phase appears to develop via intermediate sodium-rich $(K_{1-x}Na_x)NbO_3$ and $K_4Nb_6O_{17}$ phases. This is probably due to the difference in diffusion rate and reactivity between Na^+ and K^+ ions. A single phase $(K_{0.5}Na_{0.5})NbO_3$ powder with tetragonal structure and a mean grain size of ~ 30 nm could be prepared at a calcination temperature of 650 °C. This method allows the formation of $(K_{0.5}Na_{0.5})NbO_3$ nano powder at temperatures 100 ~ 300 °C lower than that of conventional solid state reaction routes and without the need for ball milling the starting materials using organic solvents.

Acknowledgements

This research was supported by the Basic Science Research Program through the National Research Foundation of Korea (NRF), funded by the Ministry of Education under Grant number: 2015R1D1A1A01057060. The authors would like to thank Kyeong-Kap Jeong and Jeong-Chi Sang (Centre for Research Facilities, Chonnam National University) for operating the XRD and FTIR, Hey-Jeong Kim (Centre for Development of Fine Chemicals, Chonnam National University) for operating the SEM and Dr. Sang-Hun Jeong and Kang-Min Lee (Korea Basic Science Institute, Gwangju centre) for carrying out the Raman scattering and slow-scan XRD experiments respectively.

References

1. J. Rödel, W. Jo, K.T.P. Seifert, E.-M. Anton, T. Granzow, and D. Damjanovic, J. Am. Ceram. Soc. 92[6] (2009) 1153-1177.
2. J. Rödel, K.G. Webber, R. Dittmer, W. Jo, M. Kimura, and D. Damjanovic, J. Eur. Ceram. Soc. 35[6] (2015) 1659-1681.
3. B. Malič, J. Koruza, J. Hreščak, J. Bernard, K. Wang, J. Fisher, and A. Benčan, Materials 8[12] (2015) 5449.
4. J. Wu, D. Xiao, and J. Zhu, Chem. Rev. 115[7] (2015) 2559-2595.
5. M. Villafuerte-Castrejón, E. Morán, A. Reyes-Montero, R. Vivar-Ocampo, J.A. Peña-Jiménez, S.O. Rea-López, and L. Pardo, Materials 9[1] (2016) 21.
6. K. Wang, B. Malič, and J. Wu, MRS Bulletin 43[8] (2018) 607-611.
7. H.-C. Thong, C. Zhao, Z. Zhou, C.-F. Wu, Y.-X. Liu, Z.-Z. Du, J.-F. Li, W. Gong, and K. Wang, Materials Today 29 (2019) 37-48.
8. H. Birol, D. Damjanovic, and N. Setter, J. Eur. Ceram. Soc. 26[6] (2006) 861-866.
9. J.G. Fisher, D. Rout, K.S. Moon, and S.J.L. Kang, J. Alloys Compd. 479[1–2] (2009) 467-472.
10. J. Hreščak, A. Bencan, T. Rojac, and B. Malič, J. Eur. Ceram. Soc. 33[15–16] (2013) 3065-3075.
11. N. Marandian Hagh, B. Jadidian, and A. Safari, J Electroceram 18[3-4] (2007) 339-346.
12. J. Koruza, A.J. Bell, T. Frömling, K.G. Webber, K. Wang, and J. Rödel, J. Materiomics 4[1] (2018) 13-26.
13. H.-C. Thong, C. Zhao, Z.-X. Zhu, X. Chen, J.-F. Li, and K. Wang, Acta Mater. 166 (2019) 551-559.
14. H.-C. Thong, Z. Xu, C. Zhao, L.-Y. Lou, S. Chen, S.-Q. Zuo, J.-F. Li, and K. Wang, J. Am. Ceram. Soc. 102[2] (2019) 836-844.
15. H. Yang, Y. Lin, F. Wang, and H. Luo, Mater. Manuf. Processes 23[5] (2008) 489-493.
16. A. Chowdhury, S. O'Callaghan, T.A. Skidmore, C. James, and S.J. Milne, J. Am. Ceram. Soc. 92[3] (2009) 758-761.
17. A.D. Handoko, and G.K.L. Goh, Green Chem. 12[4] (2010) 680-687.
18. G. Stavber, B. Malič, and M. Kosec, Green Chem. 13[5] (2011) 1303-1310.
19. Y. Hou, C. Wang, J. Zhao, H. Ge, M. Zhu, and H. Yan, Mater. Chem. Phys. 134[1] (2012) 518-522.
20. D.-Q. Zhang, D.-W. Wang, H.-B. Zhu, X.-Y. Yang, R. Lu, B. Wen, W.-Q. Cao, J. Yuan, and M.-S. Cao, Ceram. Int. 39[5] (2013) 5931-5935.
21. R. López-Juárez, R. Castañeda-Guzmán, and M.E. Villafuerte-Castrejón, Ceram. Int. 40[9, Part B] (2014) 14757-14764.
22. A.B. Haugen, F. Madaro, L.P. Bjørkeng, T. Grande, and M.A. Einarsrud, J. Eur. Ceram. Soc. 35[5] (2015) 1449-1457.
23. X. Meng, W. Wang, H. Ke, J. Rao, and Y. Zhou, Materials Science and Engineering: B 212 (2016) 1-6.
24. S. Toyama, H. Hayashi, M. Takesue, M. Watanabe, and R.L. Smith, J. of Supercritical Fluids 107 (2016) 1-8.
25. Y. Wang, Q. Zhang, L. Hu, E. Yu, and H. Yang, J. Alloys Compd. 685 (2016) 1-7.
26. G.H. Khorrami, M. Mousavi, and M. Dowran, Mod. Phys. Lett. B 31[15] (2017) 1750175.
27. R. Rani, S. Sharma, M. Quaglio, R. Rai, S. Bianco, D. Pugliese, and C. Pirri, Mat. Sci. Applications 8[3] (2017) 247-257.
28. N. Senes, A. Iacomini, N. Domingo, S. Enzo, G. Mulas, S. Cuesta-Lopez, and S. Garroni, Physica Status Solidi (a) 215[16] (2018).
29. H.-l. Cheng, J. Xiao, P. Gao, Y.-y. Yan, S.-p. Gao, and H.-l. Du, Transactions of Nonferrous Metals Society of China 28[9] (2018) 1801-1807.
30. S.L. Skjærvø, K.H. Wells, W. van Beek, T. Grande, and M.-A. Einarsrud, CrystEngComm 20[42] (2018) 6795-

6802.
31. B. Chen, P. Liang, D. Wu, X. Zhao, X. Qiao, Z. Peng, L. Wei, X. Chao, and Z. Yang, Powder Technol. 346 (2019) 248-255.
32. T. Su, Y. Zhai, H. Jiang, and H. Gong, Res. Chem. Intermed. 36[5] (2010) 565-575.
33. F.F.P. Medeiros, M.F.V. Moura, A.G.P. da Silva, C.P. Souza, K.K.P. Gomes, and U.U. Gomes, Brazil. J. Chem. Eng. 23 (2006) 531-538.
34. T.T. Su, Y.C. Zhai, H. Jiang, and H. Gong, J. Therm. Anal. Calorim. 98[2] (2009) 449-455.
35. H. Jiang, T.T. Su, H. Gong, and Y.C. Zhai, Cryst. Res. Technol. 46[1] (2011) 85-89.
36. I. Nowak and M. Ziolek, Chem. Rev. 99[12] (1999) 3603-3624.
37. V.S. Braga, J.A. Dias, S.C.L. Dias, and J.L. de Macedo, Chem. Mater. 17[3] (2005) 690-695.
38. B. Malic, D. Jenko, J. Bernard, J. Cilensek, and M. Kosec, Mat. Res. Soc. Proc. 755 (2002) 83-88.
39. J. Hreščak, B. Malič, J. Cilenšek, and A. Benčan, J. Therm. Anal. Calorim. 127[1] (2017) 129-136.
40. J.V. Reis, T.C.P. Pereira, T.H.A. Teles, A.B. França, J.D.A. Bellido, F.L. Naves, and E.P. Baston, Mater. Lett. 227 (2018) 261-263.
41. S. Joshi, S. Kalyanasundaram, and V. Balasubramanian, Appl. Spectrosc. 67[8] (2013) 841-845.
42. T. Ikeya and M. Senna, J. Non-Cryst. Solids 105[3] (1988) 243-250.
43. K.I. Peterson and D.P. Pullman, J. Chem. Educ. 93[6] (2016) 1130-1133.
44. L. Monico, F. Rosi, C. Miliani, A. Daveri, and B.G. Brunetti, Spectrochim. Acta Pt. A: Mol. Biomol. Spec. 116 (2013) 270-280.
45. T. Rojac, M. Kosec, P. Šegedin, B. Malič, and J. Holc, Sol. Stat. Ionics 177[33] (2006) 2987-2995.
46. B.M. Gatehouse, S.E. Livingstone, and R.S. Nyholm, J. Chem. Soc. (Resumed) (1958) 3137-3142.
47. G. Busca and V. Lorenzelli, Mat. Chem. 7[1] (1982) 89-126.
48. S.J.L. Kang, in "Sintering: Densification, Grain Growth & Microstructure" (Elsevier Butterworth Heineman, 2005) pp. 39-55.
49. R.M. German, in "Sintering Theory and Practice" (Wiley, 1996) pp. 67-141.
50. G. Rez, Y. Sakka, T.S. Suzuki, T. Uchikoshi, and E.F. Aglietti, J. Ceram. Soc. Jpn. 117[1364] (2009) 470-474.
51. M. Mazaheri, M. Valefi, Z.R. Hesabi, and S.K. Sadrnezhaad, Ceram. Int. 35[1] (2009) 13-20.
52. C. Wang, Y.-D. Hou, H.-Y. Ge, M.-K. Zhu, and H. Yan, J. Eur. Ceram. Soc. 29[12] (2009) 2589-2594.
53. D. Jenko, A. Bencan, B. Malic, J. Holc, and M. Kosec, Microsc. Microanal. 11[6] (2005) 572-580.
54. K. Kakimoto, K. Akao, Y.P. Guo, and H. Ohsato, Jpn. J. Appl. Phy. 44[9B] (2005) 7064-7067.
55. Y. Shiratori, A. Magrez, and C. Pithan, Chem. Phys. Lett. 391[4–6] (2004) 288-292.
56. N. Klein, E. Hollenstein, D. Damjanovic, H.J. Trodahl, N. Setter, and M. Kuball, J. Appl. Phys. 102[1] (2007) 014112.
57. B. Jaffe, W.R. Cook, and H. Jaffe, in "Piezoelectric Ceramics" (Academic Press, 1971) pp. 185-212.
58. B. Malic, D. Jenko, J. Holc, M. Hrovat, and M. Kosec, J. Am. Ceram. Soc. 91[6] (2008) 1916-1922.